*Proceedings of the XIII International Conference "Ion Implantation and Other Applications of Ions and Electrons"*

# Variable Energy Positron Beam Studies of Gold Exposed to $Au^+$ and $H^+$ Implantation

P. Horodek[a,*], K. Siemek[a], M.N. Mirzayev[b,c], E.P. Popov[d,e], A.A. Donkov[e], M. Kulik[f], M. Turek[f] and M. Bielewicz[g]

[a] *Institute of Nuclear Physics, Polish Academy of Science, Krakow PL-31342, Poland*
[b] *Institute of Radiation Problems, Azerbaijan National Academy of Sciences, Baku, AZ1143, Azerbaijan*
[c] *Azerbaijan State Oil and Industry University, Scientific-Research Institute Geotechnological Problems of Oil, Gas and Chemistry, AZ1010 Baku, Azerbaijan*
[d] *Institute for Nuclear Research and Nuclear Energy, Bulgarian Academy of Sciences, Sofia, 1784, Bulgaria*
[e] *Georgi Nadjakov Institute of Solid State Physics, Bulgarian Academy of Sciences, 1784, Sofia, Bulgaria*
[f] *Institute of Physics, Maria Curie-Skłodowska University, Pl. Marii Curie-Skłodowskiej 1, 20-031 Lublin, Poland*
[g] *National Centre for Nuclear Research, Otwock-Świerk, Poland*

Doi: 10.12693/APhysPolA.142.702 *e-mail: pawel.horodek@ifj.edu.pl

The results of Doppler broadening of the annihilation line spectroscopy obtained using a variable energy positron beam for the pure gold samples exposed to 100 keV self-implantation and 250 keV $H^+$ implantation are reported. The annihilation characteristics of parameter $S$ as a function of positron energy were determined. Irradiation-induced defects were confirmed in all measured profiles. However, the $S$ parameter distributions were not typical for the ion-implanted materials. No significant changes in the shape of defect profiles for non-defected and self-implanted samples were found. The implanted $Au^+$ ions fill the earlier produced vacancies and decrease the overall defect concentration. In the case of 100 keV $H^+$ implantation, the distribution does not cover the area with higher $S$ values pointing out the presence of defects. This is caused by the localization of $H^+$ inside the produced vacancies. The thicknesses of the damaged layers are smaller compared to those numerically predicted by the SRIM implantation ranges. The long-range effect was not observed.

topics: positron beam, defects, hydrogen, ion implantation

## 1. Introduction

Recently, ion beam modification of materials (IBMM) has become a common research trend. Energetic ions introduce irreversible changes in the structure through doping and the formation of lattice defects. The great variety of ion-induced effects in the materials offers the possibility for diverse research in many contexts. For example, exposition to irradiation results in the formation of a large number of structural defects causing, e.g., swelling, hardening, creep, and embrittlement [1]. As a consequence, faster wear appears. For this reason, ions can be used to simulate the impact of irradiation conditions on material properties. On the other hand, IBMM can be used to modify material properties as requested. It was proved that the presence of vacancies effectively improves the hydrogen absorption rate in palladium [2]. Ions are a simple way to produce these vacancies with a given concentration at a well determined depth. Another interesting goal of the studies is an investigation of the long-range effect involving the presence of irradiation-induced defects far behind the implanted area [3, 4].

The all mentioned aspects share a common feature — irradiation-induced damages. It is well known that structural defects have a direct impact on numerous material properties, such as hardness [5], electrical resistivity [6], thermal attributes [7], etc. A method suitable for the detection of open-volume defects as vacancies, their clusters, dislocations, and voids, is positron annihilation spectroscopy (PAS). Experimental PAS techniques make it possible to determine the concentration of the defect, evaluate the defect profile and recognize the type/size of the defect (only in the case of the positron lifetime measurements) [8, 9]. Recently, technical progress has enabled the construction of

variable energy positron (VEP) beams [10]. These devices are a useful tool for investigating defects located near the surface at depths ranging from single angstroms up to a few micrometres (depending on the positron energy and the density of the studied target).

The VEP results obtained for pure gold samples exposed to self-implantation and $H^+$ implantation are reported in this paper. Gold is a shiny metal, very popular in jewellery. It is also readily used in electronics, building, dentistry, or the space industry due to its numerous functional properties. The literature is not rich in reports regarding the defects in pure gold. For example, Nguyen et al. [11] provided experimental evidence for the volume contraction of gold implanted with a small dose of hydrogen. Zuccon et al. [12] showed the effect of decreasing overall reflectance with increasing total fluence of low-energy $He^+$ implanted into gold mirrors. In gold samples irradiated with an electron energy of 0.5–2 MeV, the existence of vacancy clusters preceded by the generation of dislocations was observed [13]. Chisholm et al. [14] found dislocation loops and stacking fault tetrahedra (SFTs) associated with individual ion strikes in gold exposed to the dual-beam self-ion irradiation of 2.8 MeV $Au^{4+}$ and 10 keV $He^{1+}$. SFTs with vacancies were created in gold after the implantation of $Xe^+$ and $Ar^+$ ions at higher temperatures [15]. Also, SFTs were recognized in gold irradiated with swift heavy ions [16]. Nitrogen ions with energies of 0.5–2 keV implanted into gold caused the formation of gold nitrides on the surface of the sample [17].

The goal of this paper was the evaluation of defect profiles and damaged layers in pure gold samples exposed to 100 keV self-implantation and 200 keV $H^+$ implantation. The characteristics of positron annihilation will be analysed.

## 2. Experimental details

### 2.1. Sample preparation

Gold samples, purchased from Goodfellow, with a purity of 99.99% and dimensions of $10\times10\times1$ mm$^3$ were measured. Annealing was then performed at 700°C for four hours under vacuum conditions of $10^{-5}$ Torr. After that, the samples were cooled down to room temperature in a closed furnace. In this way, specimens containing only residual defects were obtained. A set of six samples was prepared.

### 2.2. Ion implantation

Ion implantation was performed with the UNIMAS implanter [18]. The proton beam scanned each sample across a 5 cm square side. The ion current density did not exceed $1 \times 10^{-6}$ A/cm$^2$. Implantation was performed at room temperature with an accuracy of ±3°. The samples were treated in pairs. The first pair was implanted with the 250 keV $Au^+$ ions, and the second one with the 100 keV $H^+$ ions. The total fluence in both cases was $3 \times 10^5$ ions/cm$^2$. The ion distribution profiles simulated with SRIM/TRIM [19] are shown in Fig. 1.

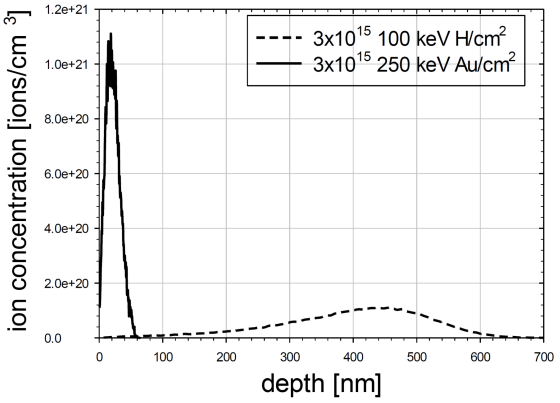


Fig. 1. Ion depth distributions for the studied samples obtained with SRIM/TRIM [19].

### 2.3. VEP measurements

The VEP measurements were performed using a positron beam with an intensity of about $10^6 e^+$/s. A positron energy ranging between 0.1 keV and 34 keV was used. According to the formula

$$\overline{z} = \frac{A\,E^n}{\rho}, \tag{1}$$

the region investigated by VEP varied from 1Å to 500 nm [20], where $\overline{z}$ is the mean implantation depth, $E$ is the positron energy, $A = 6.73$ $\mu$g/(cm$^2$ keV$^n$) and $n = 1.408$ are the Makhov's parameters, and $\rho$ is the density equal 19.30 g/cm$^3$. However, for the estimation of the implantation range, as well as for the analysis of VEP results, other parameters proposed by Vehanen et al. [21] ($A = 4$ $\mu$g/(cm$^2$ keV$^n$), $n = 1.6$, $m = 2$) are commonly used. They are constant for all materials, and the implantation depth evaluated with these parameters depends only on the density of the material. In turn, the factors from [20] are specific to a given type of medium, and for this reason, they were used in these studies. The implantation depth calculated with the parameters from [21] is smaller compared to the standard ones and equals 584 nm. On this basis, the values of positron diffusion lengths obtained from the VEP results can be changed, but the overall tendency should be preserved.

In the VEP experiment, the method of Doppler broadening (DB) of annihilation gamma line was applied. The high purity germanium (HPGe) detector with the energy resolution of 1.1 keV for 511 keV was used. The DB spectra were analysed by extracting the $S$ and $W$ parameters typical for this technique. The first parameter is given by the ratio of the area under the central part of the 511 keV line

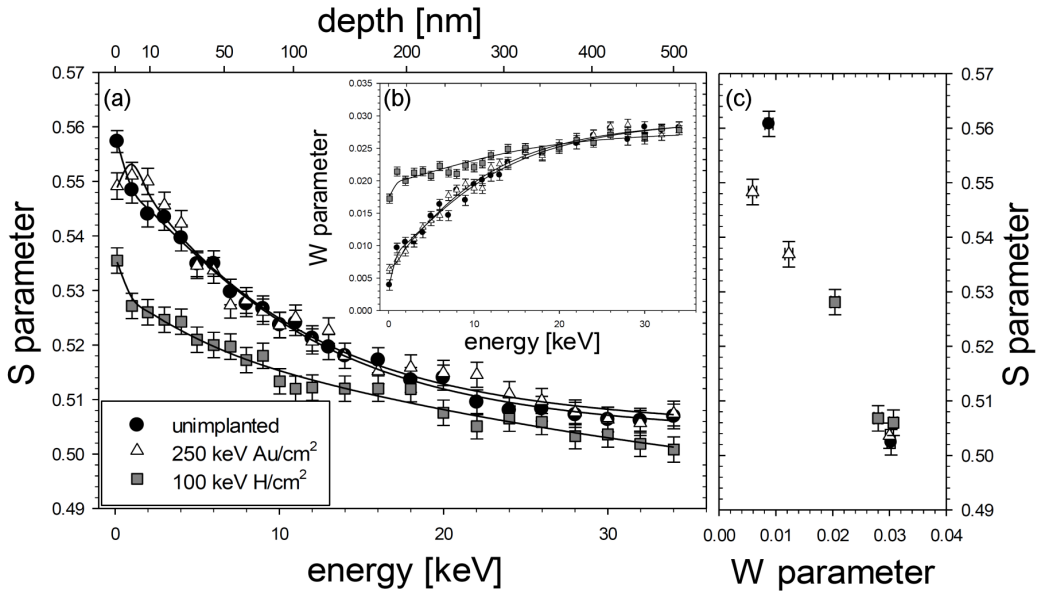


Fig. 2. The measured parameter $S$ (a) and parameter $W$ (b) as a function of the positron incident energy for the studied samples. The top axis in (a) represents the mean positron implantation depth. The solid lines represent the best fit of the experimental points using the VEPFIT code. The $W$ parameter versus the $S$ parameter is obtained from VEPFIT [27] fitting in (c).

to the total area below this peak. This feature determines the participation of the positron–electron pairs with low momentum. They are located mostly at open-volume defects. In turn, the $W$ parameter, defined as the area below the wing part of the 511 keV line to the whole area below the peak, evaluates the contribution of high momentum pairs. In reference to the data reported in this paper, it gives limited information about the type of defects.

## 3. Results and discussion

The values of the $S$ and $W$ parameters obtained from the VEP measurements are presented as a function of the positron incident energy in Fig. 2. The top axis of Fig. 2a represents the mean implantation depth obtained from (1). Black circles symbolise the reference, unimplanted sample, white triangles — self-implanted specimen, and grey squares — $H^+$ implanted one. Overall, the $S$ parameter decreases with increasing positron energy and then saturates. In the case of the reference sample, this is a feature typical of this kind of material [16]. The uneven shapes of the profiles are attributed to the back diffusion of positrons and their annihilation on the surface; hence, the higher values of the $S$ parameter at the beginning of the profiles. The $S$ parameter profile representing the self-implanted sample almost covers the distribution for the reference sample. However, in the region up to 4 keV, the values are slightly higher. Higher values of the $S$ parameter can point out the presence of irradiation-induced defects. It should be mentioned that the increase of the $S$ parameter in the damaged zone is not as clear as it was observed in the $H^+$ implanted iron. [22] The reason for this behaviour can be ascribed to the type of ions. In the case of self-implantation, other displaced or injected Au atoms can effectively fill previously produced vacancies. This results in a decreasing vacancy concentration.

Even more startling is the behaviour of the $S$ parameter distribution for the $H^+$ implanted sample. In this case, the $S$ parameter values for lower positron energies are much lower compared to the unimplanted specimen. This is a surprising behaviour because a rather intensive increase of the $S$ parameter would be achieved, especially since the range of ion implantation was much deeper compared to the previous case. According to the SRIM calculations presented in Fig. 1, the implanted depth is comparable with that studied by VEP. In [22], the profiles for the $H^+$ implanted iron were characterized by a fast $S$ parameter saturation for much higher values of the $S$ parameter compared to the defect-free ion sample. On the other hand, the decrease of the $S$ parameter can reflect the location of hydrogen inside the vacancy. The literature reports this kind of behaviour in the fcc metals like Pd, Cu, and Al [21–26]. Moreover, a similar profile of the $S$ parameter was observed by Pentecoste et al. [27] for the He implanted tungsten. According to these authors, the accumulation of He inside the W lattice induces displacement of the W atoms to form vacancies in which He is trapped. It should be emphasized that both the hydrogen and helium atoms have only fast $1s$ electrons in their electronic configuration.

In Fig. 2b, the values of the parameter $W$ versus the positron incident energy for all studied samples are shown. The presented dependencies of $W(E)$ are the reflection of the $S(E)$ profiles in terms of the abscissa. In this way, the $W$ parameter increases with the increasing positron energy, until saturation at higher energies. The opposite feature compared to $S(E)$ can be explained as follows. In the case of annihilation in defects, a higher fraction of positrons annihilate with low-momentum electrons, raising the value of the parameter $S$ and simultaneously reducing the value of the parameter $W$ representing annihilation with core electrons.

Using the VEPFIT code [28] to fit the model function to the $S(E)$ and $W(E)$ distributions made their further analysis possible. Makhov's parameters for Au, available in [20], were taken into account. Solid black lines in Fig. 2a and 2b represent the best fits. In the case of the reference sample, a single-layer model was analysed. There, the positron diffusion length $L_+$ was equal to $106 \pm 9$ nm. In the previous VEP studies of gold, the value $84 \pm 3$ nm was reported. Lakshmanan et al. [29] obtained 120 nm for well-annealed nonporous gold. Generally, positron diffusion lengths reported for defect-free metals are close to 100 nm [30]. In turn, for implanted samples, a two-layered model was assumed, composed of implanted/defected and undefected layers. In the second layer, $L_+$ was fixed (106 nm), while all other parameters were freely fitted. The positron diffusion lengths for the implanted samples were $11 \pm 2$ nm and $83 \pm 7$ nm for the self-implantation and $H^+$ implantation, respectively. The thickness of the damaged layer was $28 \pm 4$ nm for Au implantation and $477 \pm 23$ nm for $H^+$ implantation. On the basis of the following formula, $L_+$ is strictly related to the defect concentration [31] as

$$C_\nu = \frac{1}{\tau_{\text{bulk}}\mu}\left[\left(\frac{L_{\text{bulk}}}{L_+}\right)^2 - 1\right], \qquad (2)$$

where $\mu$ is the trapping coefficient typical of a given type of defect, $\tau_{\text{bulk}}$, $L_{\text{bulk}}$, and $L_+$ mean the positron lifetime, the diffusion length in the non-defected and the defected structures, respectively. In this way, the conclusion that the self-implanted layer is more defected compared to the H-implanted layer could be drawn. On the other hand, the trapping coefficients for defects induced by $Au^+$ and $H^+$ implantation should be different, and a direct comparison is not proper. Smaller values of $L_+$ for the self-implanted sample are caused by a greater number of positrons trapped at defects during the back diffusion. However, the fact that the same fluence of ions was distributed in very shallow depths should be taken into account. It should also be mentioned that the thicknesses of the damaged layers are slightly smaller compared to the SRIM calculations. This situation could have been affected by the application of Makhov's parameters from [20]. In addition, the existence of the long-range effect, which was discussed in Sect. 1, is definitely excluded on the basis of the presented studies. Further parameters $S$ and $W$ (representing "surface", "layer", and the bulk of profiles) obtained by fitting with the code VEPFIT [27] are presented in Fig. 2c. A common slope for all samples is not possible. Probably this indicates different kinds of defects.

## 4. Conclusion

VEP studies of the self-implanted and $H^+$ implanted samples were reported. In both cases, the defects profiles obtained had rather unexpected characteristics. Almost invisible changes in the distribution profile for 250 keV $Au^+$ ions could be explained by the specific kind of implantation and the shallow damaged layer. However, in the case of 100 keV $H^+$ implantation, the registered distribution points to the localization of $H^+$ inside the produced vacancies. The thicknesses of the damaged layers are smaller compared to those predicted numerically by the SRIM implantation ranges.

## References


[1] G.S. Was, *Fundamentals of Radiation Materials Science: Metals and Alloys*, 2nd ed., Springer-Verlag, New York 2017.

[2] H. Abe, H. Uchida, Y. Azum, A. Uedono, Z.Q. Chen, H. Itoh, *Nucl. Instrum. Methods Phys. Res. B* **206**, 224 (2003).

[3] P. Budzynski, *Nucl. Instrum. Methods B* **342**, 1 (2015).

[4] K. Siemek, J. Dryzek, M. Mitura-Nowak, A. Lomygin, M. Schabikowski, *Nucl. Instrum. Methods Phys. Res. B* **465**, 73 (2020).

[5] Y.A. Chang, L.M. Pike, C.T. Liu, A.R. Bilbrey, D.S. Stone, *Intermetallics* **1**, 107 (1993).

[6] S. Kobayashi, Y. Mizumukai, T. Ohnishi, N. Shibata, Y. Ikuhara, T. Yamamoto, *ACS Nano* **9**, 10769 (2015).

[7] G. Jiang, J. He, T. Zhu, Ch Fu, X. Liu, L. Hu, X. Zhao, *Adv. Funct. Mater.* **24**, 3776 (2014) .

[8] F. Tuomisto, I. Makkonen, *Rev. Mod. Phys.* **85**, 1583 (2013).

[9] K. Siemek, A.P. Yelisseyev, P. Horodek, S.I. Lobanov, A.A. Goloshumova, A.V. Belushkin, L.I. Isaenko, *Opt. Mater.* **109**, 110262 (2020).

[10] P. Horodek, A.G. Kobets, I.N. Meshkov, A.A. Sidorin, O.S. Orlov, *Nukleonika* **60**, 725 (2015).

[11] K.T. Nguyen, K.T. Nguyen, V.H. Vuong, T.N. Nguyen, T.T. Nguyen, T.Yamamoto, N.N.t Hoang, *Nat. Commun.* **12**, 1560 (2021).

[12] S. Zuccon, E. Napolitani, E. Tessarolo, P. Zuppella, A.J. Corso, F. Gerlin, M. Nardello, M.G. Pelizzo, *Opt. Mater. Express* **5**, 176 (2015) .

[13] N. Yoshida, M. Kiritani, *J. Phys. Soc. Jpn.* **35**, 1418 (1973).

[14] C. Chisholm, K. Hattar, A.M. Minor, *Mater. Trans.* **55**, 422 (2014).

[15] S. Ishino, N. Sekimura, K. Hirooka, T. Muroga, *J. Nucl. Mater.* **141–143**, 776 (1986).

[16] P. Horodek, *Vacuum* **421**, 164 (2019).

[17] L. Šiller, M.R.C. Hunt, J.W. Brown, J.-M. Coquel, P. Rudolf, *Surf. Sci.* **513**, 78 (2002).

[18] M. Turek, S. Prucnal, A. Drozdziel, K. Pyszniak, *Nucl. Instrum. Methods Phys. Res. B* **269**, 700 (2011).

[19] J.F. Ziegler, *Ion Implantation Science and Technology*, Academic Press, New York 1988.

[20] J. Dryzek, P. Horodek, *Nucl. Instrum. Methods Phys. Res. B* **266**, 4000 (2008).

[21] A. Vehanen, K. Saarinen, P. Hautojärvi, H. Huomo, *Phys. Rev. B* **35**, 4606 (1987).

[22] P. Horodek, M. Kulik, *Nucl. Instum. Methods Phys. Res. B* **443**, 84 (2019).

[23] L. Semidey-Flecha, C. Ling, D.S. Sholl, *J. Membr. Sci.* **362**, 384 (2010).

[24] L. Kristinsdóttir, E. Skúlason, *Surf. Sci.* **606**, 1400 (2012).

[25] E.V. Gómez, S. Amaya-Roncancio, L.B. Avalle, D.H. Linares, M.C. Gimenez, *Appl. Surf. Sci.* **420**, 1 (2017).

[26] B.E.F. Constance, B.K. Rao, *Rev. Adv. Mater. Sci.* **5**, 17 (2003).

[27] L. Pentecoste, A.L. Thomann, P. Brault, T. Lecas, P. Desgardin, T. Sauvage, M.F. Barthe, *Acta Materialia.* **141**, 47 (2017).

[28] A. Van Veen A, H. Schut, M. Clement, A. Kruseman, M.R. Ijpma, J.M.M. De Nijs, *Appl. Surf. Sci.* **85**, 216 (1995).

[29] C. Lakshmanan, R. N. Viswanath, R. Rajaraman, S. Dash, G. Amarendra, C.S. Sundar, *Europhys. Lett.* **117**, 48007 (2017).

[30] R. Paulin, R. Ripon, W. Brandt, *Phys. Rev. Lett.* **31**, 1214 (1973).

[31] W. Qiang-mao, S. Guo-gang, W. Rong-shan, D. Hui, P. Xiao, Z. Qi, L. Jing, *Nucl. Instrum. Methods Phys. Res. B* **287**, 148 (2012).